Available online at www.sciencedirect.com
ScienceDirect
Journal of Molecular Graphics and Modelling 25 (2007) 644–657
Journal of Molecular Graphics and Modelling
www.elsevier.com/locate/JMGM

Comparison of homology models and X-ray structures of the nuclear receptor CAR: Assessing the structural basis of constitutive activity

Björn Windshügel [a,*], Johanna Jyrkkärinne [b], Jenni Vanamo [b], Antti Poso [c], Paavo Honkakoski [b], Wolfgang Sippl [a]

[a] *Institute of Pharmaceutical Chemistry, Martin-Luther-University Halle-Wittenberg, Wolfgang-Langenbeck-Str. 4, 06120 Halle (Saale), Germany*
[b] *Department of Pharmaceutics, University of Kuopio, Harjulantie 1, P.O. Box 1627, 70211 Kuopio, Finland*
[c] *Department of Pharmaceutical Chemistry, University of Kuopio, Harjulantie 1, P.O. Box 1627, 70211 Kuopio, Finland*

Received 10 December 2005; received in revised form 28 April 2006; accepted 2 May 2006
Available online 10 May 2006

Abstract

The constitutive androstane receptor (CAR) possesses an intrinsic basal activity whose structural basis has been analysed during the last decade. Recently, we published a homology model of the CAR ligand binding domain (LBD) based on the X-ray structures of the closely related pregnane X (PXR) and vitamin D (VDR) receptor. A detailed analysis of the homology model and molecular dynamics (MD) simulations afforded us to propose a potential mechanism underlying the constitutive activity of CAR. Almost simultaneously, X-ray structures of human and mouse CAR LBD were released. In the present study, a detailed analysis and comparison of homology model and X-ray structures is carried out in order to evaluate the quality and reliability of our homology modelling procedure. The hypothesis of the constitutive activity which we proposed on the basis of our modelling results was tested for consistency with the crystal structures. In addition, the features stated to be essential for the basal activity based on the X-ray data were investigated by means of molecular dynamics simulations. Our results show that the homology modelling procedure was able to predict the CAR LBD structure with high accuracy. Structural features that have been revealed as critical for constitutive activity in the model are also observed in the X-ray structures. Furthermore, the MD simulations of the CAR X-ray structures and a detailed analysis of other NRs clarify the role of distinct structural features that have been assigned an important role for the constitutive activity.

Keywords: CAR; Constitutive androstane receptor; Docking; GROMACS; Homology modelling; Molecular dynamics; Nuclear receptor

1. Introduction

As ligand-dependent transcription factors, nuclear receptors (NRs) are involved in many physiological processes including development, differentiation, reproduction and metabolism [1]. Binding of small ligands such as steroid and thyroid hormones, fatty and bile acids, as well as retinoids induces gene expression of specific enzymes through a complex cascade culminating in modulation of the histone acetylation status and transcription rate of target genes.

The structural assembly of NRs is modular consisting of a variable N terminus, a central DNA binding domain (DBD) and a C-terminal ligand binding domain (LBD) [2]. From X-ray data the three-dimensional architecture of the DBD as well as

Abbreviations: AF-2, activation function 2; CAR, constitutive androstane receptor; CITCO, 6-(4-chlorophenyl)imidazo[2,1-*b*][1,3]thiazole-5-carbaldehyde *O*-(3,4-dichlorobenzyl)oxime; GR, Glucocorticoid receptor; LBD, ligand binding domain; LBP, ligand binding pocket; MD, molecular dynamics; NR, nuclear receptor; NRID, nuclear receptor interaction domain; PDB, Protein Databank; PXR, pregnane X receptor; RMSD, root mean square deviation; ROR, retinoid acid-related orphan receptor; RXR, retinoid X receptor; SD, steepest descent; SRC-1, steroid receptor coactivator-1; TCPOBOP, 1,4-bis[2-(3,5-dichloropyridyloxy)]benzene; TR, thyroid hormone receptor; TIF2, transcriptional intermediary factor 2; TMPP, Tri-*p*-methylphenyl phosphate; VDR, vitamin D receptor; vdW, van der Waals

* Corresponding author. Tel.: +49 345 55 25043; fax: +49 345 55 27355.
E-mail address: bjoern.windshuegel@pharmazie.uni-halle.de (B. Windshügel).

1093-3263/$ – see front matter © 2006 Elsevier Inc. All rights reserved.
doi:10.1016/j.jmgm.2006.05.002

the LBD is known [3–5]. The LBD shows a conserved folding pattern consisting of 12–14 helices arranged in a three-layered helix sandwich and a β-sheet composed of two to five strands [6]. Ligands are bound in a mainly hydrophobic ligand binding pocket (LBP) located between the outer layers of the helix sandwich. Size and shape of the LBP varies between different NRs ranging from 220 $Å^3$ (ERR3) to 1300 $Å^3$ (PPARγ) [7,8]. An exception is NURR1 which shows no LBP [9]. Besides the binding pocket, the LBD also carries the ligand dependent activation function 2 (AF-2) located on the C-terminal helix 12 (H12). The position and conformation of this helix is modulated by agonist and antagonist binding and it defines the type of co-regulator binding that are necessary for transcriptional regulation. Co-regulators encompass coactivators such as steroid receptor coactivator-1 (SRC-1) and corepressors (e.g. SMRT) which bind nearby helix 12 and are responsible for the recruitment of additional proteins necessary for gene regulation. Agonists induce H12 to cover and seal the LBP. The emerging hydrophobic surface composed of helices H3, H4 and H12 enables coactivator binding via specific aliphatic amino acid residues. A ''charge clamp'' formed by highly conserved lysine (H3) and glutamate (H12) residues stabilises the coactivator binding by interacting with the coactivator's nuclear receptor interaction domain (NRID) [7]. Binding of antagonists or inverse agonists results in transformation of H12 into a disordered conformation disrupting the coactivator binding site, thus enabling corepressor recruitment [10].

The nuclear hormone receptor superfamily comprises 48 members in human. For some NRs, the function or endogenous ligands are yet unknown. Therefore, these NRs are designated as ''orphan'' receptors [11]. CAR belongs to the sub-family NR1I of the nuclear hormone receptor superfamily including the vitamin D (VDR, NR1I1) and the pregnane X receptor (PXR, NR1I2). CAR is part of the metabolic defense in humans. In conjunction with the closely related PXR, it regulates the expression of metabolising enzymes upon xenobiotic stress [12]. Both share a variety of ligands and regulate an overlapping set of target genes [13,14]. CAR has been shown to activate expression of cytochrome P450s (CYP3A4, 2B10, 2C9) as well as conjugating enzymes and transporters [13,15–19]. Moreover, CAR has been recently found to play a significant role in bilirubin clearance and bile acid detoxification [20–22]. In contrast to other NRs, CAR possesses a constitutive activity in absence of any ligand which can be repressed by ligands such as androstenol and androstanol [23,24]. These testosterone metabolites have been identified as endogenous ligands for CAR, thereby rendering CAR an ''adopted orphan receptor'' [24]. Only few activators of CAR are known so far, including 6-(4-chlorophenyl)imidazo[2,1-*b*][1,3]thiazole-5-carbaldehyde *O*-(3,4-dichlorobenzyl)oxime (CITCO), 5β-pregnane-3,20-dione, tri-*p*-methylphenyl phosphate (TMPP), clotrimazole and artemisinin as well as some HMG-CoA reductase inhibitors [14,25–29].

The analysis of the underlying mechanism of the CAR constitutive activity has been the objective of several studies [30–33]. In order to elucidate the structural basis for constitutive activity, we generated a CAR homology model on the basis of the X-ray structures of the closely related receptors VDR and PXR. Based on MD simulations of CAR and receptor mutants as well as considering experimental site-directed mutagenesis data, we proposed a structural model explaining the constitutive activity. We observed that the basal activity of CAR is mainly dependent on van der Waals (vdW) and hydrophobic interactions between H12 and apolar residues of the LBD [34]. Amino acids V199 (H5), Y326 (H10) and I330 (H11) were observed to interact with L343 and I346 of the helix 12. Almost simultaneously with our homology model, the X-ray structures of human (PDB code: 1XV9, 1XVP) and mouse CAR (PDB code: 1XLS, 1XNX) in complex with structurally diverse ligands were reported [35–37]. Based on these crystal data also a hypothesis for the constitutive activity has been proposed by Xu et al. [35]. VdW interactions between LBD and H12, a short helix between H11 and H12 as well as a salt bridge formed between a conserved lysine residue and the C terminus were proposed to be the key elements for maintaining the high basal activity of CAR [35,36,38]. The available X-ray data for human CAR afforded us evaluate our homology model and the suggested activation mechanism. Moreover, MD simulations of ligand-free CAR X-ray structures were carried out to evaluate the putative mechanism of constitutive activity suggested by Xu et al. [35].

2. Methods

2.1. Homology modelling

Due to the high sequence identity with CAR, the PXR and VDR structures (49 and 36% sequence identity within the LBD, respectively) represent potential templates for homology modelling. Sequences were obtained from the Swiss-Prot and TrEMBL database [39]. A sequence alignment of human CAR, PXR and VDR was carried out using CLUSTAL W [40]. The template structures (PXR: 1NRL; VDR: 1DB1) were retrieved from the Protein Databank (PDB, http://www.rcsb.org/pdb) [41–43]. To account for the structural deviations of PXR from the common NR fold, the VDR structure was used as a second modelling template. The structural model of the human CAR LBD in complex with a coactivator NRID (peptide segment from SRC-1) was built using the homology module of Insight II [44]. The resulting CAR/SRC-1 model comprised amino acids 106–348 of the CAR LBD and amino acids 682–696 of the SRC-1 NRID.

2.2. Molecular dynamics simulations

A solvent box with dimensions 6.16 nm × 6.78 nm × 5.60 nm was generated in order to perform simulations in an aqueous environment. The protonation state of each amino acid residue was adjusted according to the pK_a values in a medium of pH 7.4. Protonation states of histidines were selected manually by considering the protein environment and potential hydrogen bond partners. Water molecules were represented applying a simple point charge (SPC) model [45]. 19 Na^+ and 16 Cl^- counter-ions were added by replacing water molecules to ensure the overall neutrality of the simulated system. The total

number of atoms in the system was 21505. The model was minimised using 2000 iterations of steepest descent within the GROMOS96 force field [46]. Molecular dynamics (MD) simulations with periodic boundary conditions were performed at 310 K using GROMACS [47]. The Particle-mesh Ewald (PME) method was applied to accurately determine the long-range electrostatic interactions [48,49]. VdW interactions were considered by applying a cutoff of 0.9 nm. The timestep for the simulations was set to 1 fs. To keep the system at constant temperature a Berendsen thermostat was applied using a coupling time of 0.1 ps [50]. Constant pressure was maintained by coupling to an external bath with a reference value of 10^5 Pa, with a coupling time of 1.0 ps and an isothermal compressibility of 4.5×10^{-10} Pa^{-1}.

An equilibration period of 250 ps with constraints of 1000 kJ/mol on the backbone atoms except for the H1–H3 region (amino acids 129–157) was followed by a free MD simulation for 2.25 ns. Bonds between heavy atoms and corresponding hydrogen atoms were constrained to their equilibrium bond lengths using the LINCS algorithm [51]. MD simulations of receptor mutants of CAR/SRC-1 were carried out using the same protocol.

MD simulation of the CAR X-ray structures were carried out for PDB entry 1XVP (chains B and D). Co-crystallised SRC-1 NRIDs (chain F and H) were considered in the simulations whereas ligands were not included. The protein complexes were simulated in a solvent box with dimensions 6.11 nm × 5.16 nm × 7.43 nm (1XVP chains B and F) and 7.33 nm × 5.89 nm × 5.32 nm (1XVP chains D and H). The protonation state of amino acids and the water molecules were treated as described above. The overall neutrality of the system was ensured by adding natrium and chloride ions (19 Na^+ and 17 Cl^- ions for 1XVP chains B and F; 19 Na^+ and 16 Cl^- ions for 1XVP chains D and H) replacing water molecules. The total number of atoms in both systems was 21957 (1XVP chains B and F) and 21457 (1XVP chains D and H), respectively. The structures were minimised as described for the homology models. MD simulations were performed for 250 ps with constraints of 1000 kJ mol^{-1} on all backbone atoms. Subsequently, free MD simulations were carried out for 5 ns.

2.3. Docking studies

Docking runs for CITCO and 5β-pregnanedione were carried out using programme GOLD Version 2.2 [52]. GoldScore was chosen as fitness function. 30 independent docking runs were performed for each ligand. Resulting poses were clustered into several unique binding modes on the basis of the root mean square deviation (RMSD). Clusters showing the highest fitness score were chosen for further examination. Subsequent MD simulations were computed with the settings described above. Missing parameters for the ligands were obtained manually using the GROMOS96 topology.

Trajectories of free MD simulations were analysed using NMRCLUST [53]. Representative frames from the calculated clusters were selected and minimised within GROMACS. The stereochemical quality of the structures was evaluated using PROCHECK, ProSa and Profiles-3D [54–56].

2.4. Model evaluation

Model and X-ray structures were superimposed on their backbone atoms (N, CA, C) by performing a weighted non-linear optimisation implemented in MOE (Chemical Computing Group, Montreal, Canada) according to Shapiro et al. [57]. Amino acids contributing to the accessible surface of the LBP were identified by analysing the CAR-ligand X-ray structures within MOE. Using the automated pocket assignment procedure within MOE 29 amino acid residues were considered to be part of the LBP (see Table 3).

Figures were prepared using VMD [58] and POV-ray (http://www.povray.org).

3. Results

The structural basis of the constitutive activity of CAR has been already investigated during the last years [30,32]. From site-directed mutagenesis studies, single amino acids have been detected to be essential for the basal activity of CAR. To further unravel the structural mechanism of constitutive activity, we generated a homology model of the human CAR LBD using the X-ray structures of the related PXR and VDR as template [33]. By means of MD simulations, we proposed that the CAR basal activity is mainly achieved by specific vdW and hydrophobic interactions between helix 12 and the LBD. Particularly, Y326 emerged as a central amino acid for maintaining the basal activity. Stabilised by surrounding aliphatic and aromatic amino acid residues and a hydrogen bond with N165, the Y326 side chain shows permanent contacts with H12 that resemble agonist–H12 interactions in other NRs. Therefore, we inferred that Y326 mimics a bound receptor agonist keeping H12 in the active position even in absence of any ligand. MD simulations of CAR mutants and site-directed mutagenesis data further supported our suggested hypothesis [34]. The now available X-ray structures of the CAR LBD gave us the opportunity to assess the quality of the homology modelling and refinement procedure.

3.1. Quality of the homology model

To investigate how well the modelled structure matches the X-ray data, the CAR/SRC-1 homology model and crystal structures were superimposed on their backbone atoms (Fig. 1A). The overall arrangement of helices and loops in the model is in good agreement with the corresponding elements in the X-ray structures (see Fig. 1A and the alignment in Fig. 1B). Solely helices H3 and H10/11 show an additional turn in the homology model. The most strikingly difference is observed in the region connecting H2 and H3. Here the X-ray structures possess an additional helix (H2′) whereas the homology model contains a flexible loop (Fig. 1C). Also the orientation of the H2–H3 loop is different compared to the corresponding element in the X-ray structures.

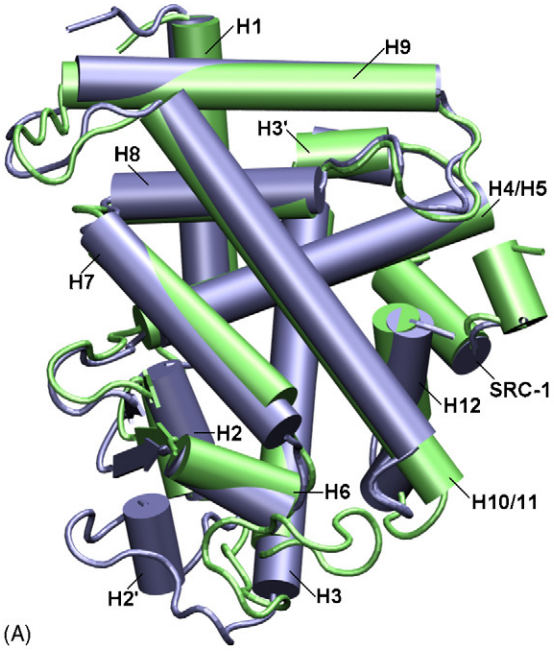

(A)

```
CAR      103   PVQLSKEQEELIRTLLGAHTRHMGTMFEQFVQFRPP------------------------------AHLF
MODEL    106     LSKEQEELIRTLLGAHTRHMGTMFEQFVQFRPP------------------------------AHLF
PXR      142    GLTEEQRMMIRELMDAQMKTFDTTFSHFKNFRLPGV|REEAAKWSQVRKDLCSLKVSLQLRGEDGSVWN
VDR      120  LRPKLSEEQQRIIAILLDAHHKTYDPTYSDFCQFRPP------------------------------VRVN

CAR      143  IHHQP-LPTLAPVLPLVTHFADINTFMVLQVIKFTKDLPVFRSLPIEDQISLLKGAAVEICHIVLNTTFCLQ
MODEL    143  IHHQP-LPTLAPVLPLVTHFADINTFMVLQVIKFTKDLPVFRSLPIEDQISLLKGAAVEICHIVLNTTFCLQ
PXR      225  YKPPA-DSGGKEIFSLLPHMADMSTYMFKGIISFAKVISYFRDLPIEDQISLLKGAAFELCQLRFNTVFNAE
VDR      161  DGGGS|VTLELSQLSMLPHLADLVSYSIQKVIGFAKMIPGFRDLTSEDQIVLLKSSAIEVIMLRSNESFTMD

CAR      215  TQNFLCG--PLRYTIEDGARVGFQVEFLELLFHFHGTLRKLQLQEPEYVLLAAMALFSPDRPGVTQRDEIDQ
MODEL    215  TQNFLCG--PLRYTIEDGARVGFQVEFLELLFHFHGTLRKLQLQEPEYVLLAAMALFSPDRPGVTQRDEIDQ
PXR      296  TGTWECG--RLSYCLEDTAG-GFQQLLLEPMLKFHYMLKKLQLHEEEYVLMQAISLFSPDRPGVLQHRVVDQ
VDR      283  DMSWTCGNQDYKYRVSDVTKAGHSLELIEPLIKFQVGLKKLNLHEEEHVLLMAICIVSPDRPGVQDAALIEA

CAR      284  LQEEMALTLQSYIKGQQRRPRDRFLYAKLLGLLAELRSINEAYGYQIQHI---QGLS-AMMPLLQEICS
MODEL    284  LQEEMALTLQSYIKGQQRRPRDRFLYAKLLGLLAELRSINEAYGYQIQHI---QGLS-AMMPLLQEICS
PXR      365  LQEQFAITLKSYIECNRPQPAHRFLFLKIMAMLTELRSINAQHTQRLLRI---QDIHPFATPLMQELFGITG
VDR      355  IQDRLSNTLQTYIRCRHPPP|--LLYAKMIQKLADLRSLNEEHSKQYRCLSFQPECSMKLTPLVLEVFGNEI
```

(B)

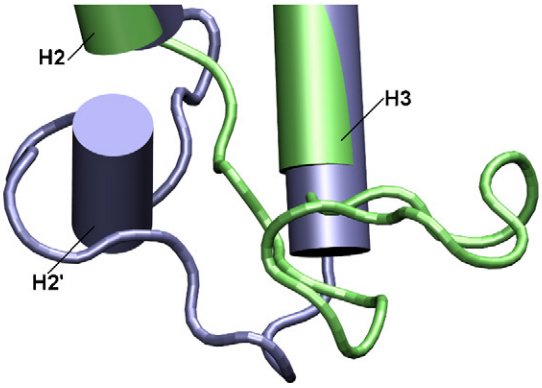

(C)

Fig. 1. Comparison of the CAR homology model and X-ray structures. (A) Superimposition of CAR/SRC-1 X-ray structure 1XVP (chains D and H, blue) and the CAR/SRC-1 homology model after free MD simulation (green) on backbone atoms (N-CA-C). Helices are depicted by cylinders, β-sheets by arrows, random-coil by tube. (B) Sequence alignment and comparison of secondary structural elements observed for the X-ray structures (CAR, PXR, VDR) and CAR homology model (MODEL). Helices are marked red whereas β-strands are marked green. (C) Detailed view of the region located between helices H2 and H3 where model and X-ray structures show the largest deviations.

Table 1
Stereochemical parameters of the CAR/SRC-1 homology model and the model-ligand complexes

Model	Un-liganded CAR model (different stages of model refinement)				CAR-ligand complexes (docking with subsequent MD)			
	1	2	3	4	CLOT	TMPP	CITCO	PREG
RMSD 1	3.4	3.4	3.6	3.7	4.4	3.4	3.8	3.9
RMSD 2	1.8	1.8	1.9	1.9	2	2	1.9	2.2
Z-score	−8.69	−9.37	−9.68	−9.44	−10.05	−9.49	−9.78	−9.63
Profiles-3D	112	111	119	116	112	115	118	115

RMSD values (Å) are average values calculated between the X-ray structures 1XV9/1XVP and the model structures at different stages of the refinement (model "1" denotes the original homology model without any refinement, model "2" is obtained after energy minimisation, model "3" indicates the structure resulting from the equilibration MD and model "4" is a representative frame of the free MD; CLOT (Clotrimazole), TMPP, CITCO and PREG (5β-pregnanedione) denotes the corresponding CAR-ligand complexes derived from MD simulations). "RMSD 1" includes all backbone atoms whereas "RMSD 2" is calculated for backbone atoms excluding the segment 139–153.

Table 2
Accuracy of LBP modelling

Model	Un-liganded CAR model (different stages of model refinement)				CAR-Ligand complexes (docking with subsequent MD)			
	1	2	3	4	CLOT	TMPP	CITCO	PREG
Backbone atoms	1.1	1.1	1.1	1	1.2	1.5	1.4	1.4
Heavy atoms	1.7	1.7	1.5	1.7	1.8	1.8	1.9	1.7

RMSD values (Å) are average values calculated between the X-ray structures 1XV9/1XVP and the model structures. For abbreviations see Table 1.

To assess the model accuracy, the RMSD values between superimposed model and crystallographic structures were calculated. RMSD values for the backbone atoms were found to vary between 3.4 and 4.4 Å suggesting a suboptimal modelling quality (see Table 1 for details). However, from a visual inspection a good overall agreement of secondary structural elements of the homology model and the X-ray structures is observed (Fig. 1A). In fact, high RMSD values originate mainly from large deviations in the H2–H3 region. Excluding this segment (amino acids 139–153) from the measurement, the RMSD dropped significantly to values between 1.8 and 2.2 Å (Table 1). Since the H2′–H3 loop is located at the protein surface and the residues located therein neither contribute to the formation of the LBP nor to the dimerisation interface it is suggested that the misprediction in this region has no major influence on the general reliability of the CAR model. This is also supported by the closely related VDR. It contains a significantly larger H2–H3 region which does not affect the main receptor function [59].

To determine the stereochemical quality of the homology model we used two approaches, ProSa2003 and Profiles-3D (Table 1) [55,56]. Combined *Z*-scores calculated with ProSa show relatively high energies for the initial model. However, they were significantly decreased in the subsequent minimisation and MD simulation. A further decrease was observed when the CAR model was simulated in the ligand-complexed form. The resulting *Z*-score is close to the values observed for the CAR X-ray structures (−9.70 to −10.05). In agreement with the ProSa result also the Profiles-3D approach shows an improvement of the model quality during the refinement process (profiles-3D scores calculated for the crystal structures range from 112 to 119).

To further evaluate the accuracy of the CAR model we compared the side chain orientations of the amino acids forming the LBP in the model and the X-ray structures. For this purpose 29 amino acids contributing to the accessible surface of the LBP were analysed. CAR model and X-ray structures were superimposed and the RMSD was calculated for backbone atoms (between 1.0 and 1.5 Å) and all heavy atoms (between 1.5 and 1.9 Å, depending on the stage of refinement) (Table 2). Fig. 2 shows the superimposed binding pockets of the homology model and the X-ray structure 1XVP illustrating the high accuracy of the CAR model. For comparison, the

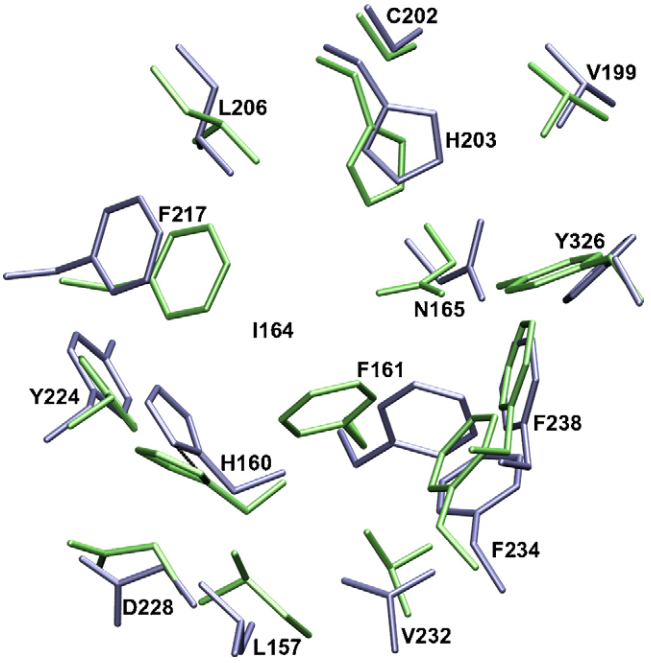

Fig. 2. Accuracy of LBP modelling. Side chain conformations of several amino acids lining the LBP. Residues of the X-ray structure (1XVP) are coloured in blue whereas amino acids of the homology model are shown in green.

RMSD values for the individual chains of the CAR X-ray structures lie in the range between 0.4 and 0.6 Å.

Besides the calculation of RMSD values also the χ_1 dihedral angles of LBP side chains were analysed and compared with those observed in the X-ray structures (Table 3). Dihedrals were considered as correctly predicted when the deviation compared to the values in the crystal structures was less than 10°. According to this criteria, about two-third of all dihedral angles were correctly predicted. The number of outliers range from 12 in the raw model to 9 in a representative frame of the free MD simulation.

In order to identify amino acids important for the constitutive activity, a variety of CAR mutants has been experimentally studied [30,32–34,60]. In order to elucidate the structural basis for the inactivity of some of these CAR mutants, we also generated models of mutated CAR and examined them by means of MD simulations [33]. The analysis of the simulations showed that a variety of amino acid residues are important to maintain the interaction between the key residue Y326 and H12. For example, a reorientation of Y326 and a loss of the interaction with H12 was observed in the simulation of the F238A as well as the F243A mutant. Both mutated receptors show no or a reduced basal activity in cell-based reporter assays which is in agreement with our prediction. In the present study, we analysed whether the results obtained for the CAR model could be reproduced for the CAR X-ray structures. For this purpose, the receptor mutants F238A and F243A modelled from the CAR X-ray structures were analysed by means of MD simulations (5.25 ns). Consistent with the observation derived from the simulations of the homology model, the MD simulation of the F238A mutant resulted in a reorientation of the Y326 sidechain (Fig. 3A). In contrast to the simulation of the F238A homology model, vdW contacts between Y326 and L343 (H12) were maintained throughout the whole simulation due to a reorientation of L343. However, the conformation of Y326 in the mutant is much less defined as in wild-type CAR indicated by a larger overall flexibility (Fig. 3B) suggesting a less stable interaction between LBD and H12. For F243A no reorientation of Y326 could be observed although the side chain flexibility is increased similar to the F238A mutant (Fig. 3B). During the MD simulations of the F243A homology model the hydrogen bond between H160 and Y224 was disrupted provoking a reorientation of the Y224 side chain into the LBP, an observation that was also observed for the F243A X-ray structure (data not shown).

3.2. Reproduction of ligand binding modes

We analysed whether the docking programme GOLD is able to correctly reproduce the binding mode of the two co-crystallised ligands 5β-pregnanedione and CITCO. For this purpose, the

Table 3
LBP dihedrals

Model	1	2	3	4	CLOT	TMPP	CITCO	PREG
F132	−71	−81	−71	−61	−62	**49**	**−56**	−71
L157	**−66**	**−79**	**−156**	**−155**	**−63**	**−150**	−175	**−156**
H160	174	−176	−176	178	**−158**	179	**−157**	−176
F161	**−55**	**−66**	**−144**	−177	−175	**−126**	−176	**−144**
I164	**−67**	**−46**	**−44**	**−50**	**−175**	**−58**	**−56**	**−44**
N165	**−74**	**−70**	−175	−167	−144	**−66**	−161	−175
M168	−70	−71	−73	−68	−84	−74	**−155**	−73
V169	172	**154**	**−62**	177	−174	−175	−174	**−62**
V199	172	165	**62**	−175	−173	−175	180	**62**
C202	**−180**	**−175**	−69	**−177**	**171**	−75	−72	−69
H203	−70	−67	−79	−77	−69	−81	−81	−79
L206	**−71**	**−79**	−168	**−46**	−162	**−57**	−164	−168
F217	−70	−69	−63	**−51**	**−87**	−70	−62	−63
C219	−53	−55	−58	−51	−55	−56	**−172**	−58
Y224	−46	−55	−59	−62	−67	**−68**	−63	−59
T225	63	70	71	76	65	68	62	71
I226	**−68**	**−57**	**−58**	−171	**−55**	−169	**−74**	**−58**
D228	−66	−55	−53	−57	−65	−69	−66	−53
G229	–	–	–	–	–	–	–	–
V232	**−61**	**54**	**66**	**69**	**67**	**63**	**64**	**66**
F234	−67	−67	−62	−65	−71	−71	−66	−62
F238	178	174	175	172	158	−177	177	175
L239	−72	−64	−62	−72	−65	−69	−72	−62
L242	**−146**	**−93**	**−55**	**−67**	−174	**−59**	−163	**−55**
F243	**−178**	**−175**	−87	**−68**	**70**	**−72**	**−160**	−87
H246	−72	−67	−85	−89	−88	−74	−84	−85
I322	**−67**	−68	**62**	−68	**59**	**−59**	**−66**	**−63**
Y326	179	−178	166	180	176	**−163**	174	166
L343	**−178**	**−170**	**−57**	**−170**	**−171**	**−67**	−78	−74
False	**12**	**12**	**10**	**9**	**10**	**13**	**9**	**9**

χ_1 dihedrals for residues lining the LBP. Values deviating more than 10° from minimum and maximum χ_1 dihedrals in CAR X-ray structures are considered as false predicted and are highlighted by bold face/underline (abbreviations see Table 1).

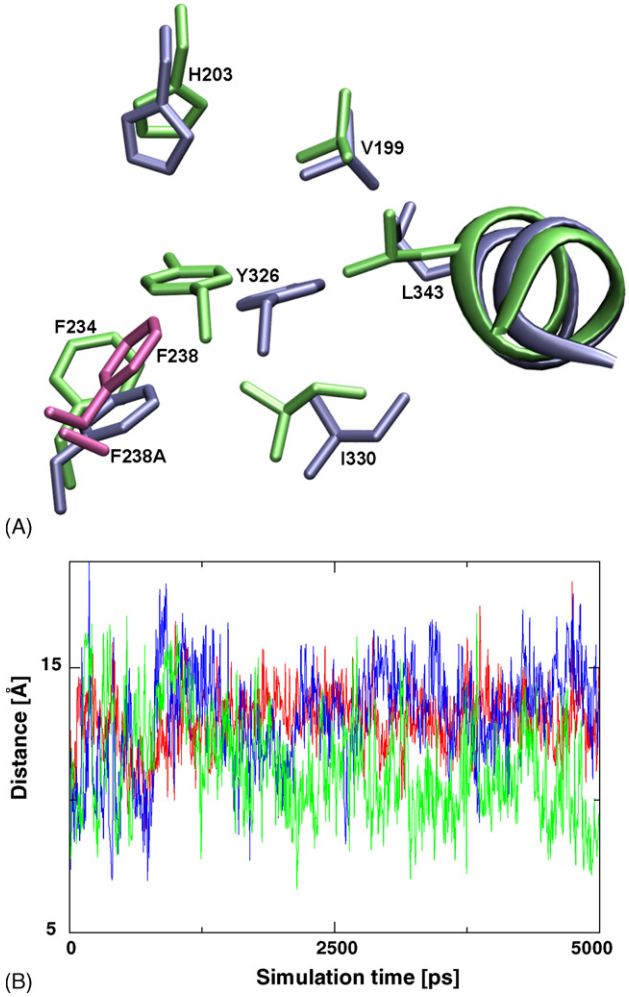

Fig. 3. Analysis of CAR receptor mutants. (A) Superimposition of CAR X-ray structure 1XVP_DH (blue) and its mutant F238A (green). Side chains of F238 and F238A are shown in pink. Helix 12 is indicated by ribbon. (B) Course of distance between Y326 (atom CZ) and L343 (atom CA) during the MD simulation for wild-type CAR (red) and mutants F238A (blue) and F243A (green).

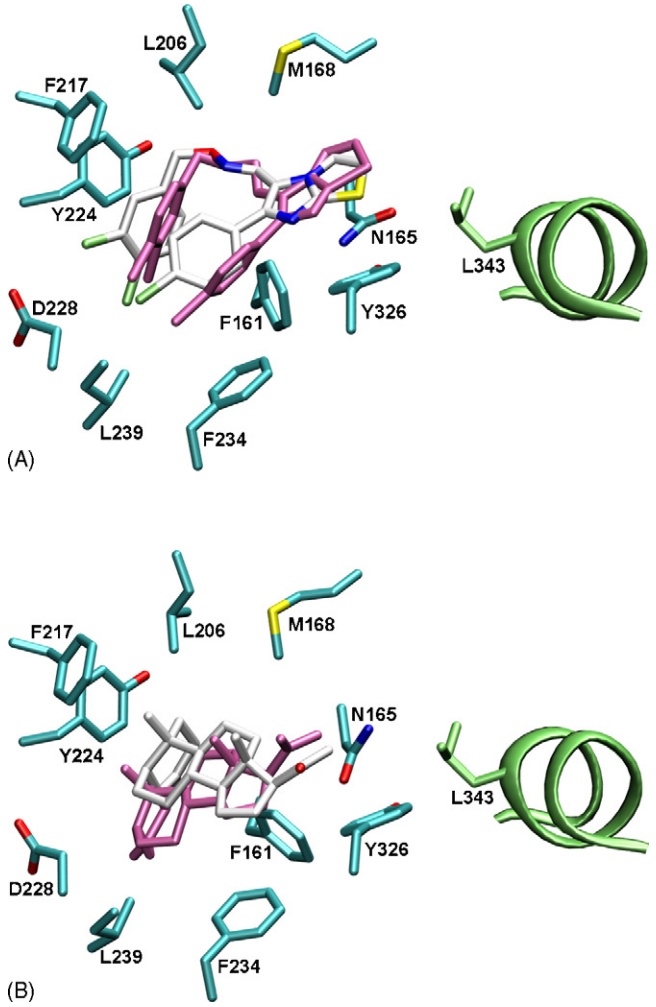

Fig. 4. Docking results. Position of (A) CITCO and (B) 5β-pregnanedione docked into the homology model in comparison with the positions observed in the X-ray structures. Carbon atoms of the co-crystallised ligands are coloured white. Docking poses are shown in pink. Helix 12 is shown as green ribbon.

ligands were first docked into the X-ray structures in order to determine how well the binding modes could be reproduced. The conformation obtained by docking is close to the experimentally observed position indicated by an RMSD of 1.48 Å for CITCO and 0.65 Å for 5β-pregnanedione. The position of CITCO docked in the homology model is almost identical to that in the crystal structures indicated by an RMSD of 1.97 Å (Fig. 4A). A subsequent MD simulation (2.25 ns) resulted in only slightly movement of CITCO within the LBP (data not shown). The experimentally determined position of 5β-pregnanedione could not be reproduced well by the GOLD docking (RMSD 4.0 Å) due to the deviated side chain conformation of Y224 in the homology model which prevents a correct placement of the ligand. To analyse whether the presence of 5β-pregnanedione will change the Y224 conformation, an MD simulation (2.25 ns) of the CAR model in complex with the docked ligand was carried out. The simulation showed a reorientation of Y224, thus leading to a orientation of 5β-pregnanedione that is consistent with the crystal structure (RMSD 2.0 Å) (Fig. 4B).

Reorientation of side chains upon ligand binding has also been observed during the MD simulation of the CAR model complexed with either clotrimazole or TMPP [33]. Two amino acids residues of the LBP emerged as highly flexible: F161 as well as Y224 were found to adopt different conformations during the simulations. The conformational flexibility of side chains facing toward the binding pocket allows the adjustment to structurally diverse ligands. MD simulations of the CAR X-ray structure in complex with 5β-pregnanedione did not show any significant side chain reorientation of F161 whereas during the simulation of ligand-free CAR X-ray F161 adopts different conformations confirming the observation from the homology model (data not shown). The other amino acids lining the LBP did not change their orientation during the MD simulations significantly.

3.3. The basis for constitutive activity

Based on the CAR crystal structures a hypothesis for the structural basis of the constitutive activity has been deduced by Xu et al. [35]. The authors stated that CAR basal activity is

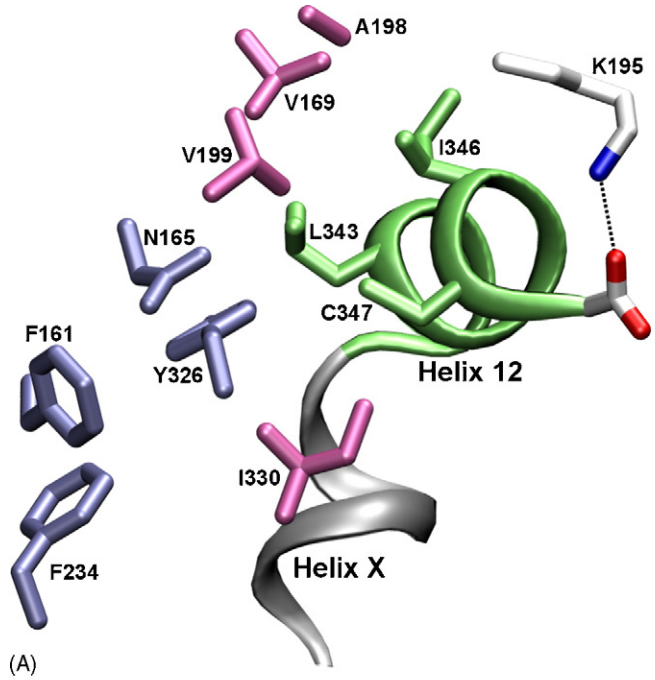

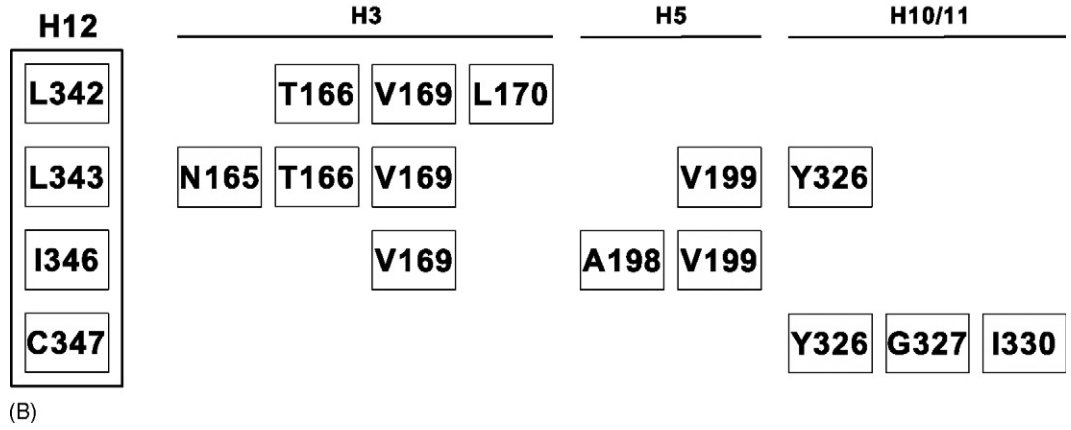

Fig. 5. Interactions between the LBD and helix H12. (A) The proposed hydrophobic barrier formed by residues N165, F161, F234 and Y326 is coloured in blue. Other residues involved in vdW interactions between LBD and H12 are coloured pink. "Helix X" is shown in grey. The salt bridge connecting H5 and the C terminus (S348) is depicted by dotted lines. H12 is shown in green. (B) Schematic view of amino acid residues contributing to vdW interactions between H12 and the residues of the LBD. For each amino acid residue located on H12 the corresponding interaction partner on helices 3, 5 and 10/11 is given.

mainly achieved by three structural features (Fig. 5A): first, a hydrophobic barrier formed by residues F161, N165, F234 and Y326 is interacting with H12 keeping it in the active conformation. Second, an additional helix (termed as "helix X") located between H11 and H12 is supposed to orient H12 in its active position and additionally contacts the hydrophobic barrier. Third, the missing C-terminal extension of H12 – observed in other NRs – is considered to allow the formation of a salt bridge between K195 on helix 5 and the C-terminal free carboxylate further stabilising the active position of H12.

We analysed the homology model if there is an agreement with the features detected in the X-ray structure. Furthermore, MD simulations of the CAR X-ray structures are used to evaluate the structural features proposed to contribute to basal activity.

A hydrophobic barrier is also existent in the homology model including Y326 as key element. Additionally, other vdW interactions between LBD and H12 can be observed in the model involving amino acids V199, I330 and I346. Further amino acids which contribute to the interaction of the LBD with H12 can be observed in the X-ray structures (Fig. 5A).

The interaction map in Fig. 5B schematically depicts all vdW contacts between amino acid residues of H12 and their corresponding interaction partners located on H3, H5 and H10/11 observed in CAR X-ray structures. Among those the influence on constitutive activity has already been confirmed for most residues by site-directed mutagenesis [30,34].

The salt bridge between K195 and S348 detected in the CAR X-ray structures (Fig. 5A) is not observed in the homology model. Instead, K195 makes a hydrogen bond to H687 located on the SRC-1 NRID whereas the C terminus (S348) interacts with Q331 on H11. The importance of Q331 for the constitutive activity has already been revealed by site-directed mutagenesis

[34]. Mutation of Q331 to alanine results in a decrease of the basal activity by about 70%. To elucidate the stability of the salt bridge in CAR X-ray structures, MD simulations (5.25 ns) of CAR/SRC-1 complexes were carried out. Ligands were removed in order to eliminate any effect on the LBD. During the simulation the salt bridge between K195 and the C terminus (S348) was found to be not stable. The distance plot clearly indicates an early separation of the two amino acids (Fig. 6A). Instead, similar to the CAR/SRC-1 homology model, K195 is involved in a hydrogen bond with H687 located on the SRC-1 NRID (Fig. 6B). Additionally, a transient hydrogen bond formation was observed between Q331 and S348 (Fig. 6C).

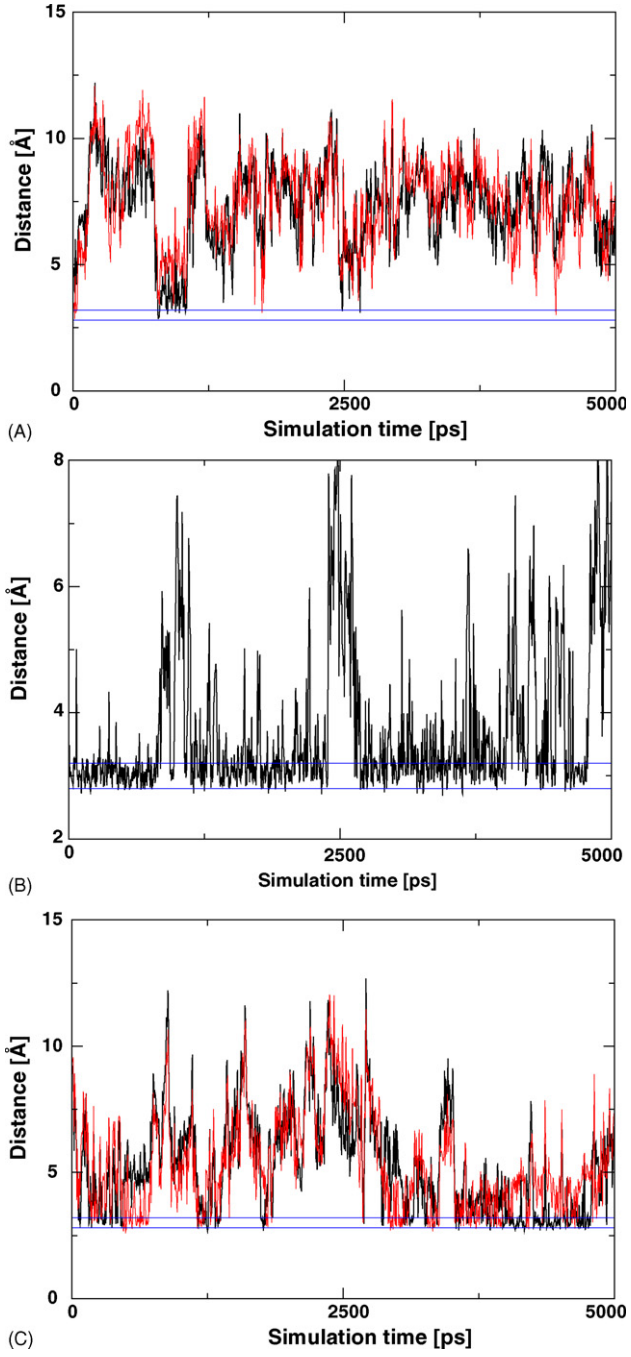

Fig. 6. Stability of the salt bridge K195–S348. Distance plots for amino acid pairs during the MD simulation. Blue lines define the area of optimum hydrogen bond and salt bridge distance, respectively. (A) Course of distance between the K195 ammonium group (atom NZ) and the C terminus. Plots are shown for both oxygens of the carboxy-terminal group (atom O1: red; atom O2: black). (B) Distance plot for the ammonium group of K195 (atom NZ) and H687 of the coactivator SRC-1 (atom NE). (C) Transient hydrogen bond formation between Q331 (atom NE2) and both oxygens of the C terminus (atom O1: red; atom O2: black).

3.4. The role of helix X

Since CAR has been crystallised only in complex with ligands and not in uncomplexed form it is not clear whether the so-called "helix X" is an essential feature for maintaining the basal activity or rather formed upon agonist binding. Therefore, we investigated the stability of the "helix X" by means of MD simulations of unliganded CAR (without coactivator NRID). During the simulation time of 10 ns the "helix X" did not show any unfolding. This is not an absolute evidence for the stability of "helix X" since helix unfolding generally occurs on a much longer time scale. However, visual inspection of a variety of NR

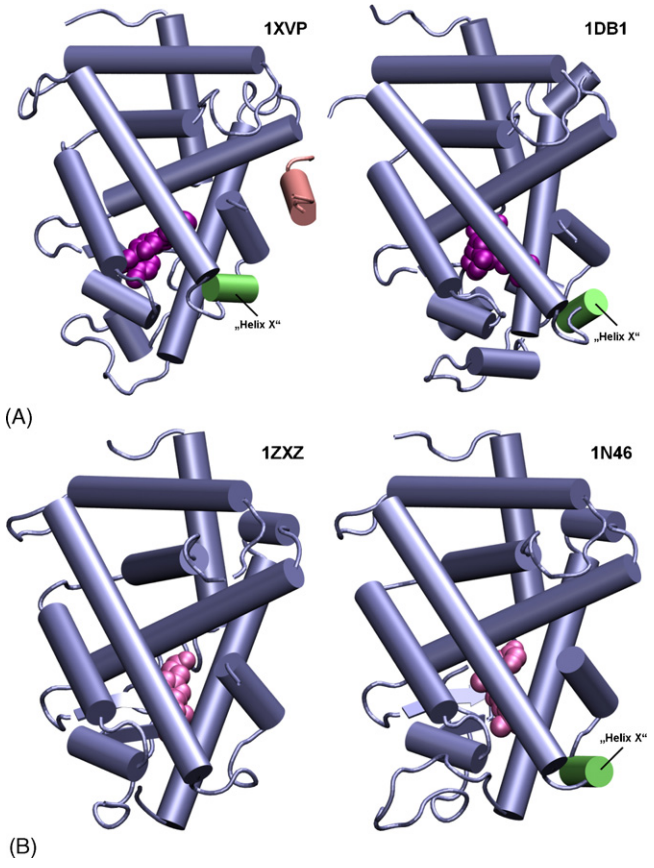

Fig. 7. Observation of the "helix X" motif in other NRs. (A) Result of the visual analysis for "helix X"-like motifs in other NRs. Besides CAR (displayed PDB entry 1XVP) also all VDR X-ray structures crystallised so far contain this helical element (displayed PDB entry 1DB1). "Helix X" is coloured green and the SRC-1 coactivator NRID is shown in pink. (B) Comparison of TRβ X-ray structures with structurally diverse ligands. In complex with T3 (Triiodothyronine) no helical structure between H10/11 and H12 is observed (PDB entry 1ZXZ), whereas in complex with a thyromimetic compound a "helix X"-like structure (coloured green) is found (PDB entry 1N46). Bound ligands are coloured magenta.

Table 4
Occurrences of helix 11′ in nuclear receptors

CAR	VDR	TRα/β	GR	RORa/β
1XV9, 1XVP, 1XLS	1DB1, 1IE8, 1IE9, 1RJK, 1RK3, 1RKG, 1RKH, 1S19, 1TXI	1N46, 1NAV, 1NAX, 1NQ0, 1NQ2, 1R6G, 1Y0X	1M2Z, 1P93	1K4W, 1N4H, 1N83, 1NQ7, 1S0X

X-ray structures (PDB entry) containing a helix 11′ (helix X) motif.

X-ray structures revealed that the ''helix X'' can also be observed among other nuclear receptors. Altogether 26 X-ray structures in the Protein Databank show a comparable helical element (Table 4). In case of VDR, which shows no basal activity, all crystal structures complexed with an agonist possess this ''helix X'' (Fig. 7A). The same holds true for the retinoid acid-related orphan receptor α and β (RORα/β). It has been speculated that in CAR the single amino acid between ''helix X'' and H12 limits the conformational freedom of H12 whereas in VDR this segment comprises two amino acids thus resulting in a larger flexibility of H12. In contrast to VDR, the segment in constitutively active ROR consists of a phenylalanine and a proline residue that has been proposed to allow only limited flexibility. However, we found that in VDR the flexibility of the segment (L414, T415) is restricted by hydrogen bonds to R154 (located on the loop connecting H2 and H3) and S235 (H3).

Another important observation is the fact that the thyroid receptor (TR) shows variability in the H11–H12 region. Among the 13 X-ray structures inspected, seven show a ''helix X''-like element whereas six do not possess an helical segment (Fig. 7B). As detected for ROR, the loop connecting ''helix X'' and H12 in TR comprises a phenylalanine and proline residue. Additionally, the C-terminal amino acid of the ''helix X'' in TR (L450) makes a hydrogen bond to T273 located on helix H3.

Another example for the observation of the ''helix X'' is the Glucocorticoid receptor (GR, 1P93). When GR is co-crystallised with dexamethasone two of the four monomers in the PDB structure show an ''helix X'' whereas the others do not.

4. Discussion

In the last few years, several homology models of CAR have been published by us and others. The models were used to analyse the structural features of the constitutive activity or the ligand binding [25,30,32,33,61,62]. Since the coordinates of the individual models have not been published a direct structural comparison is difficult. However, we tried to make a general comparison of the different CAR models (see also Table 5).

From the published data and our own results it can be stated that CAR models based on the single template PXR generally result in an overall unfavourable architecture due to the structural deviations of PXR from the common NR topology [32]. Models based on two templates represent a more sophisticated approach in which the VDR X-ray structure is used to model the problematic regions [33,61]. Refinement procedures applied during the modelling process usually result in favourable stereochemical parameters (e.g. percentage of amino acids in the most favoured region of the Ramachandran plot). This was also observed for the different stages during the refinement process of our model. However, it must be stated that this is not a measure for the agreement with crystallographic data. Another important feature of the homology models, especially if they are used for docking or structure-based drug design, is the accuracy of the binding pocket. For example, the CAR models generated by Dussault et al. and Xiao et al. were found to contain huge cavities whereas in our model the LBP is about 700 $Å^3$ smaller and much closer to the actual pocket size observed in the CAR X-ray structures (see Table 5 for details). The large difference in LBP volume is a consequence of the usage of the PXR structure as modelling template (cavity size PXR 1280–1544 $Å^3$, depending on the ligand) as well as the manual adjustment of side chain conformations [32,61].

The release of the CAR X-ray structures gave us the possibility for a detailed structural comparison of the homology model with the experimental data in order to evaluate the quality of the model. Based on the comparison, we could show that the applied modelling procedure yielded a reliable CAR model. Not only the assignment and position of the secondary structural elements are in close agreement with the X-ray data but also, more importantly, the side chain conformations of residues constituting the LBP were predicted with high accuracy. This is reflected by low RMSD values and the fraction of correctly predicted χ_1 dihedral angles. The good reproduction of the binding mode for the two agonists 5β-pregnanedione and CITCO further emphasises the high degree of consistency between model and crystallographic data.

Comparing the intermediate stages of the refinement process with the available crystallographic data revealed a slight

Table 5
Comparison of CAR homology models with available X-ray data

	Dussault et al.	Xiao et al.	Windshügel et al.	CAR X-ray	
Organism	Mouse	Human	Human	Human	Mouse
Modelling template(s)	PXR	PXR/VDR	PXR/VDR		
Ramachandran plot (% most favoured)	82.6	90	86.4	83.3–86.4	83.3–84.1
Cavity size ($Å^3$)	1150	1170	480	675	525

improvement of the model quality. Considering all calculated parameters, the CAR model derived from the constrained MD simulation is closest to the X-ray structures whereas free MD simulations decreased the model accuracy. This observation is in agreement with results obtained by Flohil et al. [63]. However, it has to be considered that CAR specific features such as the hydrogen bonds connecting N165 and Y326 as well as Q331 and S348 are not formed during energy minimisation or constrained MD, respectively.

MD simulations of CAR-ligand complexes slightly impaired the LBP accuracy in terms of RMSD, whereas the stereochemical parameters are comparable to the other models (Profiles-3D scores) or were slightly improved (ProSa *Z*-score). Results from the measurement of the χ_1 dihedral suggest that ligand binding induces a reorientation of LBP side chains in order to facilitate optimal protein–ligand interactions. This is indicated by a higher fraction of correctly predicted χ_1 dihedrals in case of CITCO and 5β-pregnanedione compared to the result obtained for TMPP and clotrimazole. However, an increased number of χ_1 outliers for TMPP does not allow to infer a worse LBP quality. Compared to CITCO and 5β-pregnanedione, TMPP is structurally different and therefore it can also be expected for this ligand that binding induces an adjustment of the side chains.

The mutational studies carried out for CAR support the hypothesis that the structural basis for the constitutive activity is mainly dependent on vdW and hydrophobic interactions between H12 and the LBD. Several vdW contacts between H12 and its interaction partners H3, H5 as well as H10/11 have also been detected in the CAR X-ray structures, where H12 is in contact with a hydrophobic segment consisting of altogether nine amino acid residues. Furthermore, the hydrogen bond between N165 and Y326 sustains the structural integrity of the LBD–H12 interface. The importance of several amino acids for constitutive activity has already been confirmed by site-directed mutagenesis studies by us and others [30,34]. Any alanine mutant reduced the basal activity dramatically. Another amino acid residue which is involved in vdW interactions with H12, V169, is a promising target for further experimental studies. We expect that the mutation of V169 to an alanine residue will also significantly reduce the constitutive activity of CAR.

Amino acids located on H12 have been already analysed by site-directed mutagenesis. The mutations L342A and L343A resulted in significantly lower basal activity which is in agreement with our theoretical observations [34]. In contrast the mutation C347A showed only slight decrease of basal activity indicating a less important role for maintaining the constitutive activity in human CAR [30]. The high sensitivity of the CAR basal activity for single point mutations indicates a relatively weak interaction of H12 with the LBD allowing an easy shift from the active into the inactive H12 conformation. This can be achieved by the introduction of single alanine mutations.

Xu et al. have discussed the role of F161 as interaction partner for the ‘‘helix X’’ and thus as component of the hydrophobic barrier [35]. From the MD simulations of the CAR homology models and X-ray structures, F161 emerged as an amino acid with high flexibility. During any MD simulations done for ligand-free CAR X-ray structures, F161 adopts a conformation pointing into the LBP and thus having no vdW interactions with ‘‘helix X’’. In contrast, in CAR complexed with the agonists CITCO or 5β-pregnanedione F161 is reoriented towards the LBD–H12 interface. In the X-ray structure of murine CAR complexed with the agonist 1,4-bis[2-(3,5-dichloro-pyridyloxy)]benzene (TCPOBOP), the corresponding F171 points into the LBP, similar to the conformation observed during MD simulations for ligand-free human CAR X-ray structures [36]. These observations clearly indicate the high flexibility of F161 and the possibility to adopt different conformations depending on the bound ligand.

Moreover, the observed flexibility of F161 might be a hint for the structural basis of activating CAR beyond its basal activity. In contrast to agonists showing direct contact with H12 (such as TCPOBOP does in murine CAR) other agonists might interact indirectly with H12 by reorienting F161 towards this helix. In this conformation, F161 is able to restrict the movement of Y326 via its bulky aromatic side chain. Results from the MD simulations show that agonist binding moves Y326 closer towards H12 in cooperation with F161 thus reinforcing vdW interactions.

We observed in the MD simulations that the salt bridge connecting K195 and the C-terminal S348 is not stable. K195 rather was found to form a hydrogen bond to H687 located on the SRC-1 NRID. The C terminus in turn has been observed to have transient interactions with Q331. Site-directed mutagenesis has already revealed the importance of Q331 for the basal activity of CAR. Experimental data concerning K195 and S348 are controversial. Andersin et al. [31] reported that extension of H12 by three residues did not influence the basal activity whereas in other studies extension of H12 resulted in loss of basal activity which has been interpreted as confirmation of the K195-C terminus interactions [30,64]. However, it cannot be excluded that elongation of H12 by one turn disrupts the potential hydrogen bond between Q331 and the C terminus leading to destabilisation of H12. Furthermore, CAR X-ray data suggests that a C-terminal extension might result in a steric clash with H5 resulting in displacement of H12 and CAR inactivation.

In another report mutation of K195 to alanine impaired binding of coactivator GRIP1 but not SRC-1 to the thyroid hormone receptor [60]. Supershift assays for CAR showed that mutation K195A disrupts the interaction of CAR with the coactivator TIF-2. Interestingly, in this experiment CITCO was able to recover the interaction with TIF-2 [30]. From the available experimental data, K195 emerges as important residue for coactivator recruitment. Whether this is achieved by direct contact with the coactivator or by keeping H12 in the active position via interacting with the C terminus is not clear so far. It cannot be excluded that K195 not only stabilises coactivator binding but simultaneously constitutes interactions with H12 as observed in the crystal structures of other NRs (e.g. PXR and PPAR).

For mouse CAR additional interactions between S337 and the C terminus have been described and discussed as being

involved in the stabilisation of the active conformation of helix H12 [36,38]. In human CAR the corresponding amino acid is glycine which is not able to interact with H12. The visual inspection of the murine CAR X-ray structure (PDB code 1XLS) also revealed no such interaction.

"Helix X" has been assigned a major role for the CAR basal activity. However, several crystal structures deposited in the Protein Databank were found to contain a corresponding helical motif and for most of them no constitutive activity has been reported. Similar helical elements in the H11–H12 region can be detected in the X-ray structures of RORα and β, TRα and β, VDR as well as GR. These observations stress the question whether the occurrence of a single turn helix can serve as an explanation for the basal activity of CAR. According to the common annotation of helices in nuclear receptors, "helix X" should be rather termed helix 11′ as it has been done at first in RORβ [65].

The flexibility in the H11′–H12 region has been used as structural explanation for the different activation profiles of CAR and RORα/β (constitutive activity) in contrast to that of VDR (no constitutive activity) [35]. However, the stated higher flexibility of the H11′–H12 region in VDR is limited by hydrogen bonds stabilising the amino acids of this segment. As described before, the loop connecting H11′ and H12 in ROR and TR is identical, but in contrast to ROR, TR activates gene expression in a ligand dependent manner and shows no constitutive activity. The additional hydrogen bond that further stabilises H11′ in TR also contradicts the hypothesis of Xu et al. that a rigid H11–H12 region is a key element for constitutive activity [35].

The occurrence of H11′ in TR (and GR) dependent on the bound ligand suggests that the formation of H11′ in TR (and GR) is modulated upon ligand binding. Whether the formation of H11′ is required for coactivator binding remains unknown and has to be examined by further studies in the future.

5. Conclusions

In this study, we could show that the applied homology modelling procedure enabled the generation of a CAR model that is in good agreement with the now available X-ray crystallographic data. Particularly, the side chain conformations of amino acids lining the LBP were predicted with high accuracy. MD simulations of the CAR model and X-ray structures revealed a high flexibility of F161 that might play a role in the adjustment to structurally diverse ligands. The salt bridge between K195 and the C terminus observed in the CAR X-ray structures was found to be unstable during MD simulations. The examination of available NR X-ray structures showed that a "helix X"-corresponding element can also be observed in receptors possessing no constitutive activity. The obtained results do not support the interpretation of helix 11′ (helix X) as an essential structural feature for CAR basal activity. The crystal structure of ligand-free CAR will clarify whether helix 11′ ("helix X") is a permanent feature or – as we predict – is rather formed upon agonist binding.

Acknowledgements

We thank Birgit Schlegel for carefully reading the manuscript and Birte Brandt (Institute for Pharmaceutical Chemistry, Heinrich-Heine University Düsseldorf, Germany) for calculating Profiles-3D scores.

References

[1] V. Laudet, H. Gronemeyer, The Nuclear Receptor Factsbook, Academic press, London, 2002.
[2] M. Robinson-Rechavi, H. Escriva Garcia, C. Laudet, The nuclear receptor superfamily, J. Cell Sci. 116 (2003) 585–586.
[3] T. Hard, E. Kellenbach, R. Boelens, B.A. Maler, K. Dahlman, L.P. Freedman, J. Carlstedt-Duke, K.R. Yamamoto, J.A. Gustafsson, R. Kaptein, Solution structure of the glucocorticoid receptor DNA-binding domain, Science 249 (1990) 157–160.
[4] B.F. Luisi, W.X. Xu, Z. Otwinowski, L.P. Freedman, K.R. Yamamoto, P.B. Sigler, Crystallographic analysis of the interaction of the glucocorticoid receptor with DNA, Nature 352 (1991) 497–505.
[5] W. Bourguet, M. Ruff, P. Chambon, H. Gronemeyer, D. Moras, Crystal structure of the ligand-binding domain of the human nuclear receptor RXR-α, Nature 375 (1995) 377–382.
[6] J.M. Wurtz, W. Bourguet, J.P. Renaud, V. Vivat, P. Chambon, D. Moras, H. Gronemeyer, A canonical structure for the ligand-binding domain of nuclear receptors, Nat. Struct. Biol. 3 (1996) 87–94.
[7] R.T. Nolte, G.B. Wisely, S. Westin, J.E. Cobb, M.H. Lambert, R. Kurokawa, M.G. Rosenfeld, T.M. Willson, C.K. Glass, M.V. Milburn, Ligand binding and coactivator assembly of the peroxisome proliferator-activated receptor-γ, Nature 395 (1998) 137–143.
[8] H. Greschik, J.M. Wurtz, S. Sanglier, W. Bourguet, A. van Dorsselaer, D. Moras, J.P. Renaud, Structural and functional evidence for ligand-independent transcriptional activation by the estrogen-related receptor 3, Mol. Cell 9 (2002) 303–313.
[9] Z. Wang, G. Benoit, J. Liu, S. Prasad, P. Aarnisalo, X. Liu, H. Xu, N.P.C. Walker, T. Perlmann, Structure and function of Nurr1 identifies a class of ligand-independent nuclear receptors, Nature 423 (2003) 555–560.
[10] A.M. Brzozowski, A.C. Pike, Z. Dauter, R.E. Hubbard, T. Bonn, O. Engstrom, L. Ohman, G.L. Greene, J.A. Gustafsson, M. Carlquist, Molecular basis of agonism and antagonism in the oestrogen receptor, Nature 389 (1997) 753–758.
[11] R.M. Evans, The steroid and thyroid hormone receptor superfamily, Science 240 (1998) 889–895.
[12] P. Wei, J. Zhang, M. Egan-Hafley, S. Liang, D.D. Moore, The nuclear receptor CAR mediates specific xenobiotic induction of drug metabolism, Nature 407 (2000) 920–923.
[13] J.M. Maglich, C.M. Stoltz, B. Goodwin, D. Hawkins-Brown, J.T. Moore, S.A. Kliewer, Nuclear pregnane X receptor and constitutive androstane receptor regulate overlapping but distinct sets of genes involved in xenobiotic detoxification, Mol. Pharmacol. 62 (2002) 638–646.
[14] L.B. Moore, D.J. Parks, S.A. Jones, R.K. Bledsoe, T.G. Consler, J.B. Stimmel, B. Goodwin, C. Liddle, S.G. Blanchard, T.M. Willson, J.L. Collins, S.A. Kliewer, Orphan nuclear receptors constitutive androstane receptor and pregnane X receptor share xenobiotic and steroid ligands, J. Biol. Chem. 275 (2000) 15122–15127.
[15] P. Honkakoski, I. Zelko, T. Sueyoshi, M. Negishi, The nuclear orphan receptor CAR responds to phenobarbital in activating the CYP2B6 gene, Mol. Cell. Biol. 18 (1998) 5652–5658.
[16] B. Goodwin, E. Hodgson, D.J. D'Costa, G.R. Robertson, C. Liddle, Transcriptional regulation of the human CYP3A4 gene by the constitutive androstane receptor, Mol. Pharmacol. 62 (2002) 359–365.
[17] S.S. Ferguson, E.L. Lecluyse, M. Negishi, J.A. Goldstein, Regulation of human CYP2C9 by the constitutive androstane receptor: discovery of a new distal binding site, Mol. Pharmacol. 62 (2002) 737–746.
[18] O. Burk, K.A. Arnold, A. Geick, H. Tegude, M. Eichelbaum, A role for constitutive androstane receptor in the regulation of human intestinal MDR1 expression, Biol. Chem. 386 (2005) 503–513.

[19] J.M. Maher, X. Cheng, A.L. Slitt, M.Z. Dieter, C.D. Klaassen, Induction of the multidrug resistence-associated protein family of transporters by chemical activators of receptor-mediated pathways in mouse liver, Drug Metab. Dispos. 33 (2005) 956–962.
[20] W. Huang, J. Zhang, S.S. Chua, M. Qatanani, Y. Han, R. Granata, D.D. Moore, Induction of bilirubin clearance by the constitutive androstane receptor (CAR), Proc. Natl. Acad. Sci. U. S. A. 100 (2003) 4156–4161.
[21] G.L. Guo, G. Lambert, M. Negishi, J.M. Ward, H.B. Brewer Jr., S.A. Kliewer, F.J. Gonzalez, C.J. Sinal, Complementary roles of farnesoid X receptor, pregnane X receptor, and constitutive androstane receptor in protection against bile acid toxicity, J. Biol. Chem. 278 (2003) 45062–45071.
[22] B. Goodwin, J.T. Moore, CAR: detailing new models, Trends Pharmacol. Sci. 25 (2004) 437–441.
[23] M. Baes, T. Gulick, H.S. Choi, M.G. Martinoli, D. Simha, D.D. Moore, A new orphan member of the nuclear hormone receptor superfamily that interacts with a subset of retinoic acid response elements, Mol. Cell. Biol. 14 (1994) 1544–1552.
[24] B.M. Forman, I. Tzameli, H.S. Choi, J. Chen, D. Simhal, W. Seol, R.M. Evans, D.D. Moore, Androstane metabolites bind to and deactivate the nuclear receptor CAR-β, Nature 395 (1998) 612–615.
[25] J.M. Maglich, D.J. Parks, L.B. Moore, J.L. Collins, B. Goodwin, A.N. Billin, C.A. Stoltz, S.A. Kliewer, M.H. Lambert, T.M. Willson, J.T. Moore, Identification of a novel human constitutive androstane receptor (CAR) agonist and its use in the identification of CAR target genes, J. Biol. Chem. 278 (2003) 17277–17283.
[26] P. Honkakoski, J.J. Palvimo, L. Penttilä, J. Vepsäläinen, S. Auriola, Effects of triaryl phosphates on mouse and human nuclear receptors, Biochem. Pharmacol. 67 (2004) 97–106.
[27] J. Mäkinen, C. Frank, J. Jyrkkärinne, J. Gynther, C. Carlberg, P. Honkakoski, Modulation of mouse and human phenobarbital-responsive enhancer module by nuclear receptors, Mol. Pharmacol. 62 (2002) 366–378.
[28] O. Burk, K.A. Arnold, A.K. Nussler, E. Schaeffeler, E. Efimova, B.A. Avery, M.A. Avery, M.F. Fromm, M. Eichelbaum, Antimalarial artemisinin drugs induce cytochrome P450 and MDR1 expression by activation of xenosensors pregnane X receptor and constitutive androstane receptor, Mol. Pharmacol. 67 (2005) 1954–1965.
[29] K. Kobayashi, Y. Yamanaka, N. Iwazaki, I. Nakajo, M. Hosokawa, M. Negishi, K. Chiba, Identification of HMG-CoA reductase inhibitors as activators for human, mouse and rat constitutive androstane receptor, Drug Metab. Dispos. 33 (2005) 924–929.
[30] C. Frank, F. Molnar, M. Matilainen, H. Lempiäinen, C. Carlberg, Agonist-dependent and agonist-independent transactivations of the human constitutive androstane receptor are modulated by specific amino acid pairs, J. Biol. Chem. 279 (2004) 33558–33566.
[31] T. Andersin, S. Väisänen, C. Carlberg, The critical role of carboxy-terminal amino acids in ligand-dependent and -independent transactivation of the constitutive androstane receptor, Mol. Endocrinol. 17 (2003) 234–246.
[32] I. Dussault, M. Lin, K. Hollister, M. Fan, J. Termini, M.A. Sherman, B.M. Forman, A structural model of the constitutive androstane receptor defines novel interactions that mediate ligand-independent activity, Mol. Cell. Biol. 22 (2002) 5270–5280.
[33] B. Windshügel, J. Jyrkkärinne, A. Poso, P. Honkakoski, W. Sippl, Molecular dynamics simulations of the human CAR ligand binding domain: deciphering the molecular basis for constitutive activity, J. Mol. Mod. 11 (2005) 69–79.
[34] J. Jyrkkärinne, B. Windshügel, J. Mäkinen, M. Ylisirniö, M. Peräkylä, A. Poso, W. Sippl, P. Honkakoski, Amino acids important for ligand specificity of the human constitutive androstane receptor, J. Biol. Chem. 280 (2005) 5960–5971.
[35] R.X. Xu, M.H. Lambert, B.B. Wisely, E.N. Warren, E.E. Weinert, G.M. Waitt, J.D. Williams, J.L. Collins, L.B. Moore, T.M. Willson, J.T. Moore, A structural basis for constitutive activity in the human CAR/RXRα heterodimer, Mol. Cell 16 (2004) 919–928.
[36] K. Suino, L. Peng, R. Reynolds, Y. Li, J. Cha, J.J. Repa, S.A. Kliewer, H.E. Xu, The nuclear xenobiotic receptor CAR: structural determinants of constitutive activation and heterodimerization, Mol. Cell 16 (2004) 893–905.
[37] L. Shan, J. Vincent, J.S. Brunzelle, I. Dussault, M. Lin, I. Ianculescu, M.A. Sherman, B.M. Forman, E.J. Fernandez, Structure of the murine constitutive androstane receptor complexed to androstenol: a molecular basis for inverse agonism, Mol. Cell 16 (2004) 907–917.
[38] D.D. Moore, CAR: three new models for a problem child, Cell. Metab. 1 (2005) 6–8.
[39] B. Boeckmann, A. Bairoch, R. Apweiler, M.C. Blatter, A. Estreicher, E. Gasteiger, M.J. Martin, K. Michoud, C. O'Donovan, I. Phan, S. Pilbout, M. Schneider, The SWISS-PROT protein knowledgebase and its supplement TrEMBL in 2003, Nucleic Acids Res. 31 (2003) 365–370.
[40] J.D. Thompson, D.J. Higgins, T.J. Gibson, CLUSTAL W: improving the sensitivity of progressive multiple sequence alignment through sequence weighting, position-specific gap penalties and weight matrix choice, Nucleic Acids Res. 22 (1994) 4673–4680.
[41] H.M. Berman, J. Westbrook, Z. Feng, G. Gilliland, T.N. Bhat, H. Weissig, I.N. Shindylov, P.E. Bourne, The protein Data Bank, Nucleic Acids Res. 28 (2000) 235–242.
[42] R.E. Watkins, P.R. Davis-Searles, M.H. Lambert, M.R. Redinbo, Coactivator binding promotes the specific interaction between ligand and the pregnane X receptor, J. Mol. Biol. 331 (2003) 815–828.
[43] N. Rochel, J.M. Wurtz, A. Mitschler, B. Klaholz, D. Moras, The crystal structure of the nuclear receptor for vitamin D bound to its natural ligand, Mol. Cell 5 (2000) 173–179.
[44] Insight II, Accelrys Inc., San Diego, CA, 2000.
[45] H.J.C. Berendsen, J.P.M. Postma, W.F. van Gunsteren, J. Hermans, in: B. Pullman (Ed.), Intermolecular Forces, Reidel, Dordrecht, 1981, pp. 331–342.
[46] W.R.P. Scott, P.H. Hünenberger, I.G. Tironi, A.E. Mark, S.R. Billeter, J. Fennen, A.E. Torda, T. Huber, P. Krüger, W.F. van Gunsteren, The GROMOS biomolecular simulation program package, J. Phys. Chem. A 103 (1999) 3596–3607.
[47] GROMACS Version 3.2.1, University of Groningen, The Netherlands.
[48] T. Darden, D. York, L. Pedersen, Particle mesh-Ewald: an *N*-log(*N*) method for Ewald sums in large systems, J. Comp. Phys. 98 (1993) 10089–10092.
[49] U. Essmann, L. Perera, M.L. Berkowitz, T. Darden, H. Lee, L.G. Pedersen, A smooth Particle mesh Ewald potential, J. Comp. Phys. 103 (1995) 8577–8592.
[50] H.J.C. Berendsen, J.P.M. Postma, A. DiNola, J.R. Haak, Molecular dynamics with coupling to an external bath, J. Chem. Phys. 81 (1984) 3684–3690.
[51] B. Hess, H. Becker, H.J.C. Berendsen, J.G.E.M. Fraaije, LINCS: a linear constraint solver for molecular simulations, J. Comp. Phys. 18 (1997) 1463–1472.
[52] GOLD Version 2.2, CCDC, Cambridge, UK.
[53] L.A. Kelley, S.P. Gardner, M.J. Sutcliffe, An automated approach for clustering an ensemble of NMR-derived protein structures into conformationally-related subfamilies, Prot. Eng. 9 (1996) 1063–1065.
[54] R.A. Laskowski, M.W. MacArthur, D.S. Moss, J.M. Thornton, Main-chain bond lengths and bond angles in protein structures, J. Appl. Cryst. 26 (1993) 283–291.
[55] M.J. Sippl, Recognition of errors in three-dimensional structures of proteins, Proteins 17 (1993) 355–362.
[56] J.U. Bowie, R. Lüthy, D. Eisenberg, A method to identify protein sequences that fold into a known three-dimensional structure, Science 253 (1991) 164–170.
[57] A. Shapiro, J.D. Botha, A. Pastore, A.M. Lesk, A method for multiple superposition of structures, Acta Crystallogr. A 48 (1992) 11–14.
[58] W. Humphrey, A. Dalke, K. Schulten, VMD: visual molecular dynamics, J. Mol. Graph. 14 (1996) 33–38.
[59] N. Rochel, G. Tocchini-Valentini, P.F. Egea, K. Juntunen, J.M. Garnier, P. Vihko, D. Moras, Functional and structural characterization of the insertion region in the ligand binding domain of the vitamin D nuclear receptor, Eur. J. Biochem. 268 (2001) 971–979.
[60] W. Feng, R.C.J. Ribeiro, R.L. Wagner, H. Nguyen, J.W. Apriletti, R.J. Fletterick, J.D. Baxter, P.J. Kushner, B.L. West, Hormone-dependent coactivator binding to a hydrophobic cleft on nuclear receptors, Science 280 (1998) 1747–1749.

[61] L. Xiao, X. Cui, V. Madison, R.E. White, K.C. Cheng, Insights from a three-dimensional model into ligand binding to constitutive active receptor, Drug Metab. Dispos. 30 (2002) 951–956.

[62] M.N. Jacobs, M. Dickins, D.F.V. Lewis, Homology modelling of the nuclear receptors: human oestrogen receptorβ (hERβ), the human pregnane-X-receptor (PXR), the Ah receptor (AhR) and the constitutive androstane receptor (CAR) ligand binding domains from the human oestrogen receptor α (hERα) crystal structure, and the human peroxisome proliferator activated receptor α (PPARα) ligand binding domain from the human PPARγ crystal structure, J. Steroid. Biochem. Mol. Biol. 84 (2003) 117–132.

[63] J.A. Flohil, G. Vriend, H.J.C. Berendsen, Completion and refinement of 3-D homology models with restricted molecular dynamics: application to targets 47, 58, and 111 in the CASP modelling competition and posterior analysis, Proteins 48 (2002) 593–604.

[64] H. Lempiäinen, F. Molnar, M. Macias Gonzalez, M. Peräkylä, C. Carberg, Antagonist- and inverse agonist-driven interactions of the vitamin D receptor and the constitutive androstane receptor with co-repressor protein, Mol. Endocrinol. 19 (2005) 2258–2272.

[65] C. Stehlin, J.M. Wurtz, A. Steinmetz, E. Greiner, R. Schule, D. Moras, J.P. Renaud, X-ray structure of the orphan nuclear receptor RORβ ligand-binding domain in the active conformation, EMBO J. 20 (2001) 5822–5831.